Electrochimica Acta 148 (2014) 46–52

Contents lists available at ScienceDirect

Electrochimica Acta

journal homepage: www.elsevier.com/locate/electacta

One-pot preparation of crystalline-amorphous double-layer structured WO_3 films and their electrochromic properties

Huiying Qu [a], Xiang Zhang [b], Lei Pan [b], Zeng Gao [a], Lihua Ma [a], Jiupeng Zhao [a,*], Yao Li [b]

[a] School of Chemical Engineering and Technology, Harbin Institute of Technology, 150001, Harbin, China
[b] Center for Composite Material, Harbin Institute of Technology, Harbin, China

ARTICLE INFO

Article history:
Received 8 April 2014
Received in revised form 13 September 2014
Accepted 4 October 2014
Available online 16 October 2014

ABSTRACT

WO_3 films with crystalline-amorphous double-layer structure were prepared via one-pot electrochemical synthesis for the first time. According to scanning electron microscopy images combined with X-Ray diffraction patterns, the crystalline layer and the amorphous layer can be distinguished. Results of electrochromic measurements show that the as-synthesized films have shorter response time than crystalline films and better durability than amorphous films. The films were then modified by electrochemical lithiation/delithiation to produce a porous surface and electrochromic behaviors (response time, coloration efficiency, etc.) were studied by controlling the current and cycle times during electrochemical lithiation/delithiation. Response time is shortened and coloration efficiency is improved after electrochemical lithiation/delithiation. The formation of color centers was also analyzed. Increasing the concentration of H^+ ions is beneficial to the formation of surface color centers, while increasing the applied current benefits the formation of body color centers.

© 2014 Elsevier Ltd. All rights reserved.

1. Introduction

Electrochromic (EC) materials, whose optical properties (transmittance, reflectance, absorptance) can be changed reversibly and persistently when applied a low-voltage signal, have been extensively studied due to their wide applications, such as information display [1,2], antidazzling rear-view mirrors [3], smart windows [4,5] and so on. As an EC material, tungsten trioxide (WO_3) has been identified as one of the most promising inorganic materials due to its outstanding physical and chemical properties, such as long term cyclic stability, short response time, high coloration efficiency (CE), large optical modulation and high initial transparency and has been extensively studied.

To select EC materials, there are two important criteria [6]: one is the response time, which is limited by the diffusion coefficient and the length of the diffusion path, the other is CE, which determines the optical modulation with charge insertion or extraction. It is well known from the literature that EC performance of the WO_3 film is closely related to the level of crystallization [7–10]. Fully crystalline WO_3 films are of dense and well-ordered structure, exhibiting slow dissolution rate in acidic electrolytes. However, they respond to applied voltages slowly due to the presence of higher energy barrier for Li^+ ions to insert, resulting in long response time and poor CE, which has remained the major unsolved problems. Amorphous WO_3 films have been demonstrated to exhibit short response time and the highest CE in the visible region [11,12], but due to structural modifications of the flexible amorphous matrix and high dissolution rate in the electrolytes, long term EC stability and repeatability are greatly affected and they are of little commercial value [6,9]. However, most of the reported WO_3 films are of single-crystallinity [13–17] (for example, W.L. Kwong et al. has prepared monoclinic WO_3 films using aqueous solutions of peroxotungstic acid in one electrochemical step), and ways to induce crystallization are either by annealing at a high temperature or by treating films at a moderately elevated temperature [2]. These films do not satisfy the requirements of long term cyclic stability, short response time and high CE, thus it is an interesting way to overcome these deficiencies by developing crystalline-amorphous double-layer structured WO_3 based EC films with short response time and high CE, and may potentially have long term cyclic stability in the electrolytes without any significant degradation of performance under applied voltages that satisfy industrial needs. To date, no reports on the crystalline-amorphous double-layer structured WO_3 films could be found yet to the best of our knowledge.

Except for the crystallinity, EC properties are also affected by the porous structure. Since the degree and speed of coloration/bleaching can be accurately measured and both of them are

* Corresponding author. Tel.: 086 451 86402345, Fax: 086 45186402345.
E-mail addresses: jpzhao@hit.edu.cn (J. Zhao), yaoli@hit.edu.cn (Y. Li).

http://dx.doi.org/10.1016/j.electacta.2014.10.017
0013-4686/© 2014 Elsevier Ltd. All rights reserved.

directly related to the corresponding EC process, WO_3 is an ideal model material to study the influence of porosity on EC properties of nanoscale metal oxides. Most synthesis strategies of nanoporous materials are based on template assisted methods, which are confined by a complex synthesis process and high cost[18,19]. New approaches, based on the intercalation/extraction of Li^+ ions, produce nanopores as a result of the stresses caused by lattice distortion, and provide new ideas for synthesizing nanoporous materials in the study of transition metal oxide films [20,21]. The mechanism of Li reactivity involves the formation and decomposition of Li_2O, accompanying the reduction and oxidation of metal nanoparticles, respectively. It has been shown that this method can enhance surface electrochemical reactivity and lead to further improvements in the performance of lithium-ion batteries [22]. Besides, Pt and RuO with large surface area and pronounced nanoporosity were successfully synthesized by this method, exhibiting better performance when used as electrocatalyst and supercapacitor electrode material, respectively [23]. Synthesis of nanoporous MnOx thin-film electrodes by electrochemical lithiation/delithiation were also reported, and their capacitive performance were significantly improved [24]. Here, we use this method to modify the crystalline-amorphous double-layer structured WO_3 films, expecting that the presence of nanopores would improve the surface area, thus a large interface between WO_3 and the electrolyte can improve the diffusion coefficient of Li^+ ions. Furthermore, the porous structure in turn partitions WO_3 into small particles, decreasing the diffusion length inside the solid [8] in order to improve the EC performance.

In this work, crystalline-amorphous double-layer structured WO_3 films have been prepared via one-pot electrochemical synthesis for the first time. An electrochemical lithiation/delithiation process is then applied to the crystalline-amorphous double-layer structured WO_3 films, which leads to a porous structure and greatly increases the surface area of the films. Response time and CE of the films are studied. The double-layered WO_3 films with porous structure exhibit significantly improved EC performance.

2. Experimental section

2.1. Preparation of the crystalline-amorphous double-layer structured WO_3 films

H_2O_2, ethanol, propylene carbonate (PC), sulfuric acid, $Na_2WO_4{\cdot}2H_2O$, $LiClO_4$ and acetone (various chemical suppliers) used in this study were reagent grade and used in the as-received condition. Indium tin oxide (ITO) substrates (1 cm × 4 cm) were ultrasonically cleaned in acetone, ethanol and deionized water for 20 min, separately.

For the electrolyte, one drop of H_2O_2 was firstly added to 8 mL of 0.125 mol/L Na_2WO_4, to which then 1 mol/L H_2SO_4 was added to obtain a total volume of 10 mL. The electrochemical synthesis of the crystalline-amorphous double-layer structured WO_3 film was carried out by using a two-electrode system with CT-3008 W as the power source. It was performed at a constant current of 2 mA for 15 min on to the ITO substrate with Pt sheet as the counter electrode. The first five-minute process is cathodic electrodeposition while the subsequent ten-minute process is electrostatic attraction. This transformation of synthesis process is mainly due to the transformation of conditions from an equilibrium state to a sol-producing state, which will be explained below. Finally, a blue-colored film was obtained. Fig. 1 is the schematic diagram of the reaction process.

2.2. Electrochemical lithiation/delithiation of the films

The electrochemical lithiation/delithiation process was carried out by using a three-electrode CHI 660D electrochemical workstation (Shanghai Chenhua Instrument Co. Ltd.). The as-deposited WO_3 film was used as the working electrode, Pt sheet as the counter electrode and saturated calomel electrode as the reference electrode. 1 mol/L $LiClO_4$/PC solution was used as the electrolyte to repeat the charge and discharge cycles under conditions of ±0.3 mA and ±0.8 mA.

2.3. Characterization

Scanning electron microscopy (SEM) images were obtained using a Hitachi S-4800 microscope. X-Ray diffraction (XRD) measurement was performed using a Rigaku D/mol/Lax-3C equipment with a sweep rate of 5°/min through a diffraction angle range of 10°–90°. EC measurements were performed using Ocean Maya 2000-Pro in combination with the CHI 660D electrochemical workstation. The system was equipped with a double-layer structured WO_3 film specimen as the working electrode, Pt sheet as the counter electrode and saturated calomel electrode as the reference electrode. Throughout this paper, electrode potentials refer to the reversible hydrogen electrode (RHE) potential scale. The transmittance of the ITO substrate in the electrolyte was used as a reference for 100% transmittance.

3. Results and discussion

The double-layer structured films before and after the electrochemical lithiation/delithiation treatment are referred to as WO_3-F and WO_3-LDF, respectively.

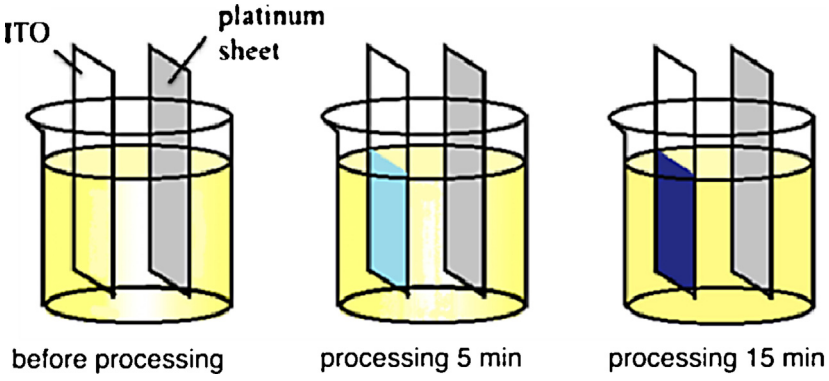

Fig. 1. Schematic diagram of the reaction process.

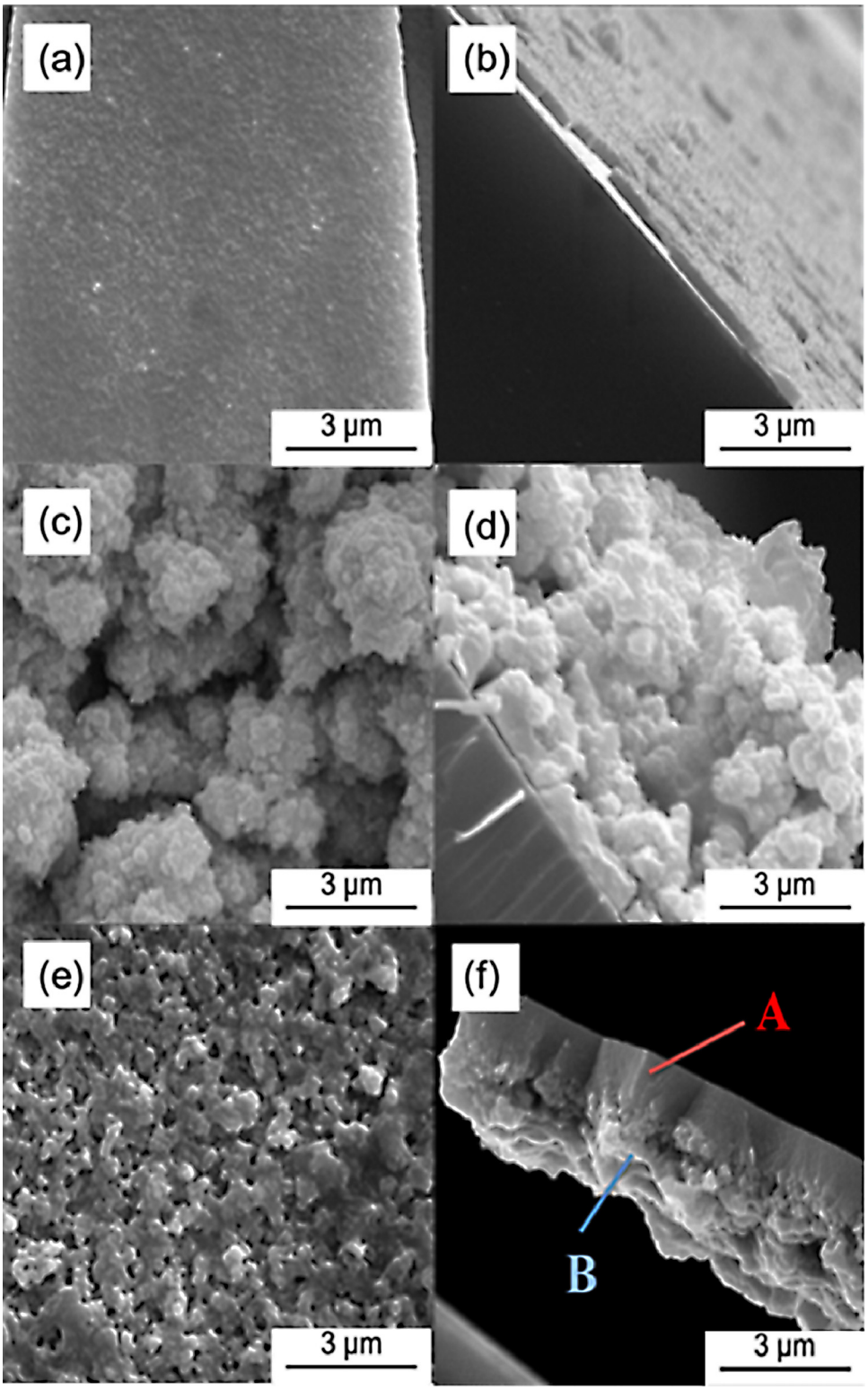

Fig. 2. SEM images of (a, b) the dense film, (c, d) the porous film, and (e, f) WO_3-F.

3.1. Morphology and phase composition of WO_3-F

After H_2O_2 was added to the electrolyte, the solution could stay stable for about 5 min. At this equilibrium state, the dense film developed under a constant current of 2 mA, as shown in Fig. 2(a) and (b).

It is believed that the anions $[W(O_2)_4]^{2-}$ are formed in mildly alkaline solution (pH 7–9) by the addition of excess H_2O_2 to solutions of $[WO_4^{2-}]$ [25] and only dimeric $[W_2(O)_3(O_2)_4(H_2O)_2]^{2-}$ species are formed in acid solutions ($pH < 5$) in a pH range where tungstic acid would lead to the precipitation of $WO_3{\cdot}2H_2O$ [26], thus $[W(O_2)_4]^{2-}$ could be formed by the addition of H_2O_2 into

Na_2WO_4. After H_2SO_4 was added, $[W_2(O)_3(O_2)_4(H_2O)_2]^{2-}$ formed according to the reaction:

$$2[W(O_2)_4]^{2-} + 5H_2O + 2H^+ \leftrightarrow [W_2(O)_3(O_2)_4(H_2O)_2]^{2-} + 4H_2O_2 \quad (1)$$

The growth of the dense film proceeded via the reduction of a peroxy-ditungstate ion ($[W_2(O)_3(O_2)_4(H_2O)_2]^{2-}$ or $W_2O_{11}{}^{2-}$) as follows:

$$W_2O_{11}{}^{2-} + (2x+6)H^+ + (2x+4)e^- \rightarrow 2H_xWO_3 + 3H_2O + O_2\uparrow \quad (2)$$

As the reaction proceeded, pH value increased due to the decrease of H^+ ions. It was observed that the electrolyte turned into a gelled sol during this process. The formation of the gelled sol could be explained as follows [26]: hydrous oxides were precipitated upon the acidification of tungstate $[WO_4]^{2-}$, around the pH where neutral precursors $[H_2WO_4]^0$ were formed. As the preferred coordination of W^{VI} is known to be mono-oxo, the neutral precursor should be $[WO(OH)_4(OH_2)]^0$. One water molecule was bonded along the z-axis opposite to the W&9552; O bond while the four OH groups were in the equatorial xy plane. Oxolation along equivalent x and y directions then leaded to the formation of the amorphous $WO_3 \bullet nH_2O$ gels. When the ITO substrate was processed in such electrolyte, $WO_3 \bullet nH_2O$ colloid particles migrated toward and were adsorbed onto the surface of the ITO substrate via electrostatic attraction. The accumulated colloid particles formed the porous film with pore sizes of about 500 nm, as shown in Fig. 2(c) and (d).

In this way, WO_3-F can be prepared during the electrolyte changing from an equilibrium state to a sol-producing state. The resulting surface morphology is shown in Fig. 2(e). From Fig. 2(f), it is clear to identify the double-layer structure: part A is the dense layer electrodeposited in the equilibrium state and part B is the porous layer formed via electrostatic attraction in the sol state.

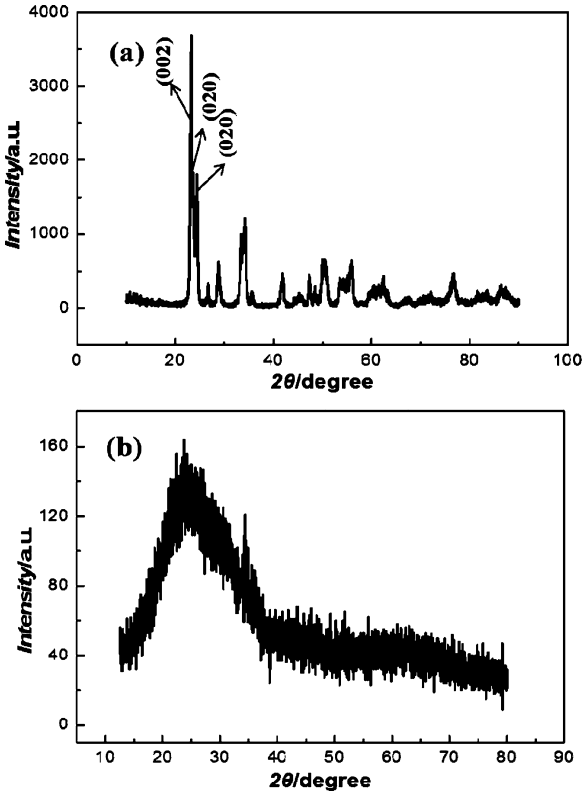

Fig. 3. XRD patterns of (a) the dense film, and (b) the porous film.

Figs. 3(a) and 3(b) show the XRD patterns of WO_3-F corresponding to Figs. 2(a) and 2(c), respectively. Fig. 3(a) is the XRD pattern of the dense film electrodeposited and all peaks are completely indexed as the monoclinic WO_3, which matches JCPDS card 72–1465. Data obtained show three major peaks at 23.1°, 23.6° and 24.4° 2θ with intensity of 100.0%, 78.3% and 97.4%, which are indexed to the (002), (020), and (200) planes, respectively. The crystallographic parameters are a = 0.7322 nm, b = 0.7509 nm, c = 0.7687 nm, α = 90.0°, β = 90.6°, γ = 90.0°. From Fig. 3(b), the films only display a broadened peak around 2θ≈25°. It indicates an amorphous WO_3 in presence, which is in accordance with the previous report [27] (for growth mechanism of WO_3-F see Fig. S1 in the Supplementary Materials, for the main elements see Fig. S2 and for electrochromism phenomenon see Fig. S3).

3.2. Influence of electrochemical lithiation/delithiation treatment on the electrochromic properties of the films

For electrochemical lithiation/delithiation, both the applied current and cycle times influence the intercalation/extraction of Li^+ ions, which has an effect on the formation of the nanopores. Thus EC performance of the films treated under different currents and cycle times were studied. Here, we modified WO_3-F with 300 lithiation/delithiation cycles at ±0.3 mA and with 500 lithiation/delithiation cycles at ±0.8 mA, represented by WO_3-LDF(1) and WO_3-LDF(2) respectively.

The response time of WO_3-F, WO_3-LDF(1) and WO_3-LDF(2) in 1 mol/L $LiClO_4$/PC was investigated by chronoamperometry(CA) measurements and the corresponding in situ coloration/bleaching transmittance response was measured at a wavelength of 800 nm with alternately applying potential of ±1 V for 60 s, as shown in Fig. 4. The measurements were performed at 25 °C. Results show

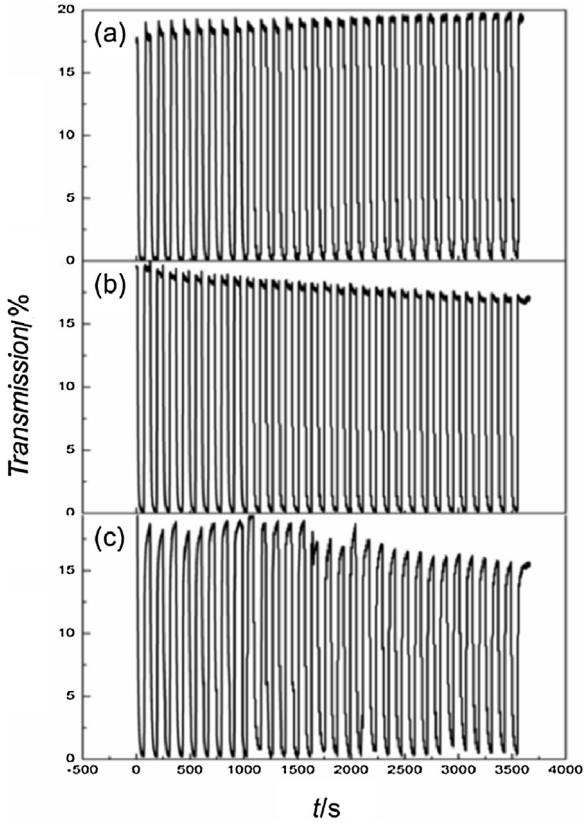

Fig. 4. Transmittance variation and response time between the colored and bleached states for (a) WO_3-F, (b) WO_3-LDF(1), and (c) WO_3-LDF(2) measured at ±1 V for 60 s with a wavelength of 800 nm in 1 mol/L $LiClO_4$/PC.

that three films display wide transmittance modulation of 20%, 17% and 15%, respectively. They retain the electrochromic properties after 500 switching cycles with little changes of optical contrast and response time (see Supplementary Materials, Fig. S4). Due to good cycle performance and conductivity of the crystalline layer, WO_3-F displays long term cyclic stability with charge reversibility of 96% (see Supplementary Materials, Fig. S5), which is higher than that of the amorphous films with charge reversibility of 93% [8]. WO_3-LDF(2) shows the worst durability of the three due to the highest internal stress in the process of lithiation/delithiation, which makes the porous structure fragile. Response time (τ_c and τ_b denote the coloration time and the bleaching time, respectively) is defined as the time required for 90% change in the full transmittance modulation. The values of τ_c and τ_b for all the films are listed in Table 1. The recorded coloration time of WO_3-F, WO_3-LDF(1) and WO_3-LDF(2) is 14.5 s, 10.3 s, and 9.2 s, and each bleaching time is 7.8 s, 6.9 s, and 6.1 s, respectively. These values are significantly shortened as compared to crystalline films with response time of almost 30 s [28], which is mainly because that the amorphous layer has low energy barrier for Li^+ ions to insert. WO_3-LDF(2) shows the shortest response time due to the most porous surface with the largest surface area and the smallest WO_3 particles. The nanopores act as the diffusion path for ions, which can improve the diffusion coefficient of Li^+ ions. The nanoparticles can signicantly decrease the diffusion length of Li^+ ions, leading to shorter response time.

Response time and CE of WO_3-F, WO_3-LDF(1), and WO_3-LDF(2) are listed in Table 1. CE was calculated using:

$$CE = OD/Q_{in} \tag{3}$$

$$OD = \lg(T_b/T_c) \tag{4}$$

$$Q_{in} = \int idt/S \tag{5}$$

Where Q_{in} is the charge intercalated; T_b and T_c represent the transmittance of the bleached and colored samples, respectively; i is the current during charge intercalating; S is the effective area of the film.

The CEs of WO_3, WO_3-LDF(1) and WO_3-LDF(2) are 9.5, 16.2, and 26.2 cm^2C^{-1}, respectively. Due to the color centers existing on the amorphous layer, these values are superior to the high-porosity crystalline films with CE [29] of 6 cm^2C^{-1}. Larger current can help Li^+ ions intercalate deeper to create more binding sites, thus WO_3-LDF(2) possesses a significantly higher CE than the other two WO_3 films do, which means that WO_3-LDF(2) can provide larger transmittance modulation via a small amount of the intercalated/extracted Li^+ ions. In general, this kind of double-layered structure can help improve EC performance of WO_3 films.

3.3. Analysis of the color center module of electrochromism

As is commonly accepted, there are absorption bands in the photochromic process of transition metal oxides [22] that can be modeled by nearly Gaussian profiles. Because electrochromism and photochromism of WO_3 are related phenomena, the color center module can be applied to both.

Surface color centers, are attributable to the formation of W^{5+}. The injected electrons and W^{6+} come together to form W^{5+}, and bonding protons to oxygen atoms by hydrogen bonds, which shows as $W^{5+}=O:H^+$. Body color centers, emerge as protons migrating from the surface to the interior, producing defects comprising W^{5+} ions and protons. Migrating protons must overcome the energy barrier either by light excitation or tunneling (under certain conditions) [2,20].

Surface color centers respond rapidly due to their coloration do not require ions diffusion, as shown in Fig. 5(a) (Peak 1). As the intercalation of H^+ ions proceeds, the number of surface color centers increases rapidly, producing significant change in the optical density (OD), particularly at high photon energies. The formation of body color centers depends on the diffusion rate of H^+ ions, hence, these color centers respond relatively slowly (Peak 2 in Fig. 5(b)), as illustrated by a comparison between Fig. 5(a) and Fig. 5(b).

The half width indicates the number of color centers, and the peak height reflects the influence of color centers on OD [30]. The fitting values of the Gaussian functions in Fig. 5(b) show that the number of body color centers (Peak 2) is larger than that of surface color centers (Peak 1), while the surface color centers have a greater influence on OD than the body color centers do. This is because that transfer of protons from the surface to the bulk phase usually happens under excitation, so the body centers start to respond after the surface color centers and thus the surface color centers have a greater influence.

Table 1
EC properties of WO_3-F, WO_3-LDF(1) and WO_3-LDF(2).

Sample	τ_c/s	τ_b/s	CE/cm^2C^{-1}
WO_3-F	14.5	7.8	9.5
WO_3-LDF(1)	10.3	6.9	16.2
WO_3-LDF(2)	9.2	6.1	26.2

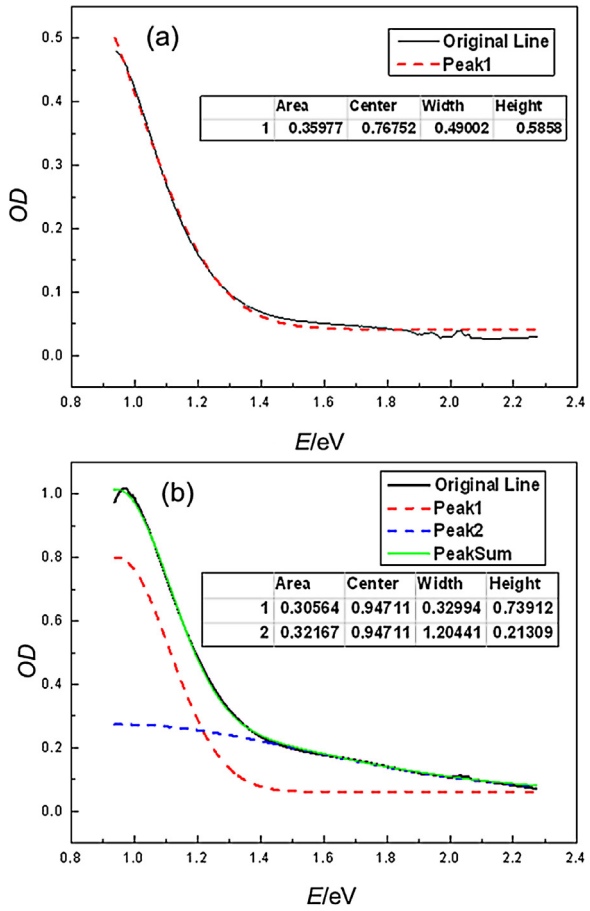

Fig. 5. Measured OD vs photon energy ("original line") and Gaussians ("peak n") of WO_3-F colored in 0.01 mol/L H_2SO_4 at a constant current of 2 mA for (a) 90 s, and (b) 8 min.

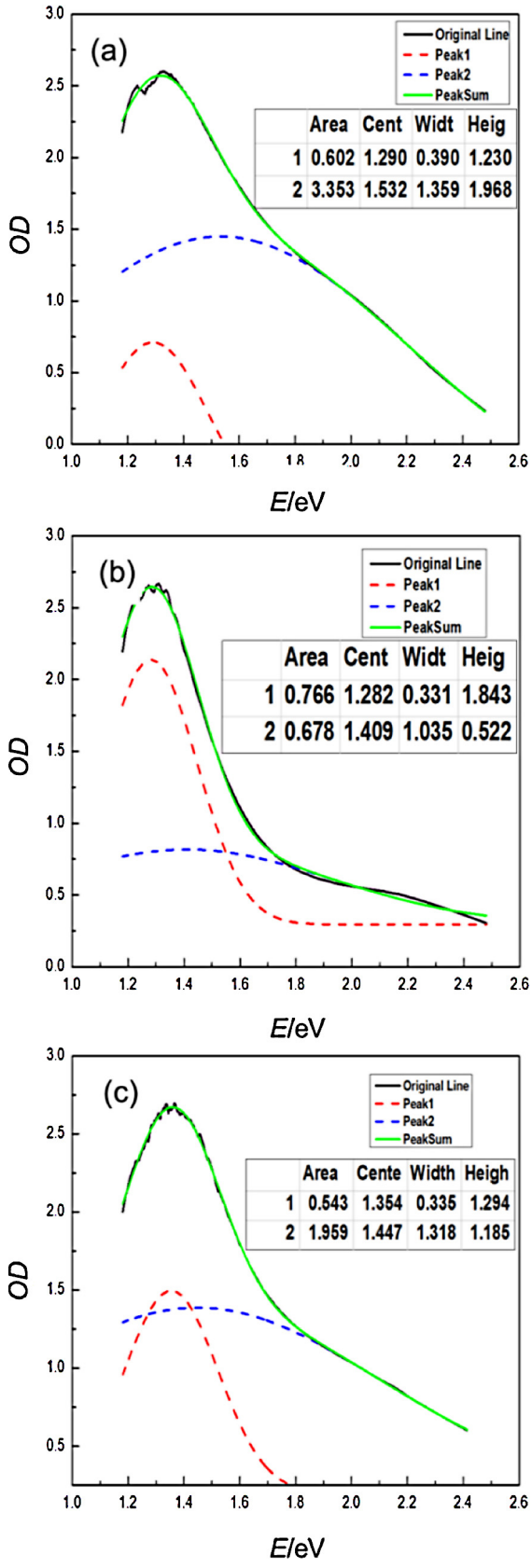

Fig. 6. OD vs. photon spectra of films and associated Gaussian fits excited under (a) a constant current of 0.8 mA in 0.01 mol/L H_2SO_4 (b) a constant current of 0.2 mA in 0.1 mol/L H_2SO_4, and (c) a constant current of 0.8 mA in 0.1 mol/L H_2SO_4.

Fig. 6 shows colored films of the deconvolution of the OD spectra into Gaussians. The results show that concentration of H^+ and applied current level influence the formation of surface color centers and body color centers. An increased concentration of H^+ ions is beneficial to the formation of surface color centers, as shown in the comparison of Fig. 6(a) and Fig. 6(c), while increasing current is beneficial to the formation of body color centers, as shown in the comparison of Fig. 6(b) and Fig. 6(c).

4. Conclusions

Results presented in this study demonstrate that the crystalline-amorphous double-layer structured WO_3 film was successfully synthesized via one-pot electrochemical method, which is of the advantages of low cost and simple technology. Because the amorphous layer has low energy barrier for ions to insert and the crystalline layer has good cycle performance and conductivity, the double-layer structured film has relatively short response time, good durability and high CE. Moreover, nanopores forming during the electrochemical lithiation/delithiation treatment lead the film with larger surface area, which can further reduce the response time and increase the CE. The films obtained under larger current and with more cycles during the lithiation/delithiation treatment exhibit shorter response time and higher CE. It is also confirmed that increasing the concentration of H^+ ions in the electrolyte is beneficial to the formation of surface color centers, while increasing current of processing is beneficial to the formation of body color centers.

Acknowledgements

We thank National Natural Science Foundation of China (No. 51010005, 91216123, 51174063), Natural Science Funds for Distinguished Young Scholar of Heilongjiang province, and the project of International Cooperation supported by Ministry of Science and Technology of China (2013DFR10630) We thank National Natural Science Foundation of China (No. 51010005, 91216123, 51174063), Natural Science Funds for Distinguished Young Scholar of Heilongjiang Province, The Natural Science Foundation of Heilongjiang Province (E201436) and the project of International Cooperation supported by Ministry of Science and Technology of China (2013DFR10630).

Appendix A. Supplementary data

Supplementary data associated with this article can be found, in the online version, at http://dx.doi.org/10.1016/j.electacta.2014.10.017.

Reference

[1] C. Marcel, J.-M. Tarascon, An all-plastic $WO_3 \cdot H_2O$/polyaniline electrochromic device, Solid State Ionics 143 (2001) 89–101.
[2] C.G. Granqvist, Handbook of inorganic electrochromic materials, Elsevier, 1995.
[3] H.J. Byker, Electrochromics and polymers, Electrochimica acta 46 (2001) 2015–2022.
[4] Z. Huang, C., Chen, L., Chaohong, S. Chen, Tungsten-doped vanadium dioxide thin films on borosilicate glass for smart window application, Journal of Alloys and Compounds, (2013).
[5] V.K. Thakur, G. Ding, J. Ma, P.S. Lee, X. Lu, Hybrid materials and polymer electrolytes for electrochromic device applications, Advanced Materials 24 (2012) 4071–4096.
[6] S.H. Lee, R. Deshpande, P.A. Parilla, K.M. Jones, B. To, A.H. Mahan, A.C. Dillon, Crystalline WO_3 nanoparticles for highly improved electrochromic applications, Advanced Materials 18 (2006) 763–766.
[7] N. Heda, B. Ahuja, Electronic properties and electron momentum density of monoclinic WO_3, Computational Materials Science 72 (2013) 49–53.

[8] S. Sallard, T. Brezesinski, B.M. Smarsly, Electrochromic stability of WO_3 thin films with nanometer-scale periodicity and varying degrees of crystallinity, The Journal of Physical Chemistry C 111 (2007) 7200–7206.
[9] H. Zheng, J.Z. Ou, M.S. Strano, R.B. Kaner, A. Mitchell, K. Kalantar–zadeh, Nanostructured tungsten oxide–properties, synthesis, and applications, Advanced Functional Materials 21 (2011) 2175–2196.
[10] J.H. Choy, Y.I. Kim, J.B. Yoon, S.H. Choy, Temperature-dependent structural evolution and electrochromic properties of peroxopolytungstic acid, Journal Of Materials Chemistry 11 (2001) 1506–1513.
[11] T. Maruyama, S. Arai, Electrochromic properties of tungsten trioxide thin films prepared by chemical vapor deposition, Journal of the Electrochemical Society 141 (1994) 1021–1024.
[12] M. Deepa, A. Srivastava, K. Sood, S. Agnihotry, Nanostructured mesoporous tungsten oxide films with fast kinetics for electrochromic smart windows, Nanotechnology 17 (2006) 2625.
[13] X. Wang, Z. Wei, C. Yu, X. Zhang, Y. Zhang, Reversible Wettability of Tungsten Trioxide Films with Novel Dandelion like Structures, Zeitschrift für anorganische und allgemeine Chemie 638 (2012) 231–235.
[14] M. Giannouli, G. Leftheriotis, The effect of precursor aging on the morphology and electrochromic performance of electrodeposited tungsten oxide films, Solar Energy Materials and Solar Cells 95 (2011) 1932–1939.
[15] S. Baeck, T. Jaramillo, G. Stucky, E. McFarland, Controlled electrodeposition of nanoparticulate tungsten oxide, Nano Letters 2 (2002) 831–834.
[16] R. Solarska, C. Santato, C. Jorand-Sartoretti, M. Ulmann, J. Augustynski, Photoelectrolytic oxidation of organic species at mesoporous tungsten trioxide film electrodes under visible light illumination, Journal of applied electrochemistry 35 (2005) 715–721.
[17] W. Kwong, N. Savvides, C. Sorrell, Electrodeposited nanostructured WO_3 thin films for photoelectrochemical applications, Electrochimica Acta 75 (2012) 371–380.
[18] L. Yang, D. Ge, J. Zhao, Y. Ding, X. Kong, Y. Li, Improved electrochromic performance of ordered macroporous tungsten oxide films for IR electrochromic device, Solar Energy Materials and Solar Cells 100 (2012) 251–257.
[19] Z. Tong, J. Hao, K. Zhang, J. Zhao, B.-L. Su, Y. Li, Improved electrochromic performance and lithium diffusion coefficient in three-dimensionally ordered macroporous V_2O_5 films, Journal of Materials Chemistry C 2 (2014) 3651–3658.
[20] A. Gavrilyuk, U. Tritthart, W. Gey, The nature of the photochromism arising in the nanosized MoO_3 films, Solar Energy Materials and Solar Cells 95 (2011) 1846–1851.
[21] J. Maier, Nanoionics: ion transport and electrochemical storage in confined systems, Nature materials 4 (2005) 805–815.
[22] P. Poizot, S. Laruelle, S. Grugeon, L. Dupont, J. Tarascon, Nano-sized transition-metal oxides as negative-electrode materials for lithium-ion batteries, Nature 407 (2000) 496–499.
[23] Y.-S. Hu, Y.-G. Guo, W. Sigle, S. Hore, P. Balaya, J. Maier, Electrochemical lithiation synthesis of nanoporous materials with superior catalytic and capacitive activity, Nature materials 5 (2006) 713–717.
[24] H. Xia, M.O. Lai, L. Lu, Nanoporous MnOx thin-film electrodes synthesized by electrochemical lithiation/delithiation for supercapacitors, Journal of Power Sources 196 (2011) 2398–2402.
[25] M.H. Dickman, M.T. Pope, Peroxo and superoxo complexes of chromium, molybdenum, and tungsten, Chemical reviews 94 (1994) 569–584.
[26] J. Livage, G. Guzman, Aqueous precursors for electrochromic tungsten oxide hydrates, Solid State Ionics 84 (1996) 205–211.
[27] T. Pauporté, A simplified method for WO_3 electrodeposition, Journal of the Electrochemical Society 149 (2002) C539–C545.
[28] S. Gubbala, J. Thangala, M. Sunkara, Nanowire-based electrochromic devices, Solar energy materials and solar cells 91 (2007) 813–820.
[29] W.T. Wu, W.P. Liao, J.S. Chen, J.J. Wu, An Efficient Route to Nanostructured Tungsten Oxide Films with Improved Electrochromic Properties, ChemPhysChem 11 (2010) 3306–3312.
[30] Ulf Tritthart, Wolfgang Gey, Alexander Gavrilyuk, Nature of the optical absorption band in amorphous H_xWO_3 thin films, Electrochimica Acta 44 (1999) 3039–3049.